# Dynamic Characteristics of the Flange Joint with a Snap in Aero-Engine

**Yu Liu, Jianjun Wang and Liqiang Chen**

*School of Energy and Power Engineering, Beihang University, Beijing 100191, China*

(Received 17 February 2017; accepted 2 February 2018)

As an important component in aero-engine, the stiffness of the flange joint has a direct impact on vibration characteristics. The paper studies the stiffness characteristics of the flange joint which includes a snap by nonlinear transient analysis in ANSYS. The angle of rotation-load curves under harmonic transverse load are obtained. It is discovered that there are different routes of curves in the process of uploading and unloading, and that the curves form a closed cycle, which is called hysteresis loop. Then, the paper also analyses the hysteresis's generation mechanism and the influence of joint parameters — preload of bolts and interference of the snap — on the shape and area of hysteresis loop. Finally, a model, which is comprised of the three-dimension finite element (namely, the joint) and beam element, is built to study the influence of hysteresis on vibration. The results show that the hysteresis of joint can be aroused under the circumstance of certain vibration amplitude and that the hysteresis can rapidly accelerate the amplitude attenuation by the mean of energy dissipation. The research results can be applied to vibration suppression design of aero-engine.

## NOMENCLATURE

**ICE** Infinitesimal Contact Element.

**Fcr** Critical Force.

## 1. INTRODUCTION

The flange joint with a snap is an important kind of joint structure, which is widely used in the rotor and stator of aero engine for its advantages: easy installation, stable performance, and good centring. Initially, the effect of joint mostly is ignored and the two parts which are combined by joint were considered as one unit; thus, the stiffness characteristics of joint were neglected. Later studies, however, discover that there is obvious stiffness loss in joint, which has great influence on vibration characteristics. As a result, many scholars start to pay attention on its stiffness characteristics and simulation.[1–3] Canyurt calculated the stiffness of the joint through genetic algorithm.[4] Wang studied the stiffness loss of the joint in aero-engine and its influence on vibration of rotor.[5] Yao presented a new dynamic modelling method which is called the improved thin-layer element method to simulate the stiffness characteristics of the joint.[6] Qin studied the Bolt loosening at rotating joint interface and its influence on rotor dynamics.[7] These researches do not take into consideration the influence of a snap on the stiffness of joint, and assume the stiffness is constant. In fact, the stiffness and contact status of the joint do vary with the loading's fluctuation. Thus, scholars studied nonlinear stiffness and energy dissipation of joint.[8–11]

Since there are several bolts distributing in the joint, the characteristic of bolted joints has a great influence on the stiffness of the joint. Existing researches point out that hysteresis appears whenthe bolt was under the transverse harmonic load.[12] Bograd studied the hysteresis for the structure with several bolts under the transverse load.[13] Qin studied axial stiffness of the interface joined by clamp band and discovered the characteristic of hysteresis.[14] Van-Long attained the hysteresis of the flange joint without a snap through the experiment.[15] Scholars focused their study on the simulation of the hysteresis.[16,17] Oldfield, Matthew used the Jenkins element to simulate the hysteresis when single bolt was under the transverse load.[18,19] Hysteresis of flange joint is caused by the shear slipping between the two parts which are combined by the bolt. But the shear slipping between the two pieces of flange is restricted by the snap and no research has ever proved whether the hysteresis exits in such a case or not.

Shuguo established the three-dimension finite element model of joint with a snap to study the stiffness characteristic under the transverse load.[20] It was found that the bending stiffness decreases suddenly once the load reaches a certain value in the process of loading and that the values of bending stiffness before and after the decrease are both constants. This phenomenon was verified by his experimental result, but no analysis of generation mechanism was conducted. In this paper, the bending stiffness of joint is studied in the process of not only loading but also unloading. The sudden decrease of stiffness is obtained again through numerical calculation. Furthermore, the joint's hysteresis, which is related to the sudden decrease of stiffness, is discovered, and the generation mechanism of the sudden decrease of stiffness and the hysteresis are studied. The paper will provide reference for vibration suppression design and analysis.

## 2. STRUCTURE AND MODEL

The main characteristics of flange joint, cylinder, nut, head of bolt, contact interface, and the snap are shown in Fig. 1a, whose structure is the same size as in the reference.[20] The snap contact interface is set as interference fit for the purpose of strict centring. The yellow lines signify contact interfaces, and contact between the screw and the bolt hole are ignored. The complete finite element model is shown in Fig. 1b; the solid parts of that model are modeled by three-dimensional brick elements called SOILD185 in ANSYS, and the contact interfaces are modelled by CONTAC174 and TARGE170. KEYOPT CNOF is set as a positive value to simulate the interfer-

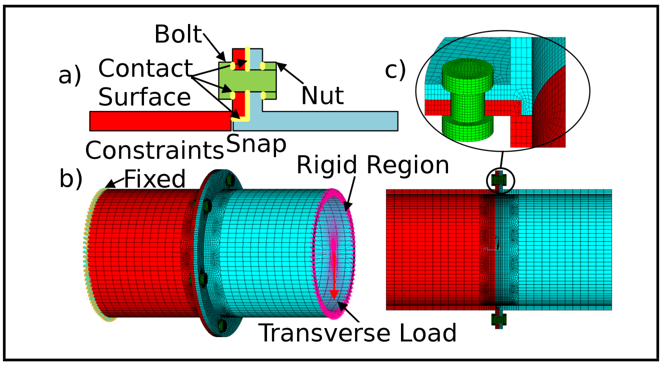


**Figure 1.** Sketch of model for the flange joint: a) sketch, b) FE model, c) details of the finite element.

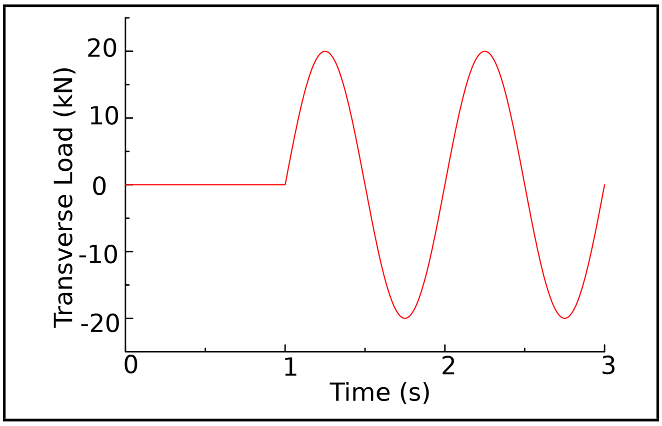


**Figure 2.** Transverse load applied on the FE model.

ence fit of the snap, and PRETS179 is used to simulate the preload of the bolt. A node which is established in the axis of the cylinder for applying cyclic loading, along with all nodes on the right edge of the cylinder is utilized to create a rigid region. Figure 1c shows the local details of the finite element mesh. The screw thread and the contact interface between nut and screw are ignored which make little difference to the stiffness of bolt. And the nut and screw are assumed as a whole.

All nodes on the left edge of the cylinder are constraint fixed. The transverse load which is applied to finite element model can be divided into two stages as is shown in Fig. 2. 0 s to 1 s indicates the first stage, in which the transverse load remains zero and the preload of bolt is applied on the element PRETS179 by use of the command of sload. Meanwhile, the time integration of ANSYS is turned off so that the preload can be applied as prestressing force of the structure. Time integration of ANSYS is turned on in the second stage from 1 s to 3 s, in which the harmonic transverse load experiences two cycles. The frequency of the harmonic transverse load is set as 1 Hz to ensure that the inertial force of the model has little influence on the result. The full transient dynamic analysis is carried out in order to take nonlinear factorsinto consideration.

This paper is to focus the research object on the angle of rotation to study the angular bending stiffness (stiffness for short) of the flange joint because the stiffness has a great influence on the transverse vibration of the structure. The data of angle of rotation is extracted from the node which is applied on the transverse load. Due to the rigid region, the angle of rotation of this node can present the rotation of the right edge of the flange joint. The transverse load is applied along Y direction

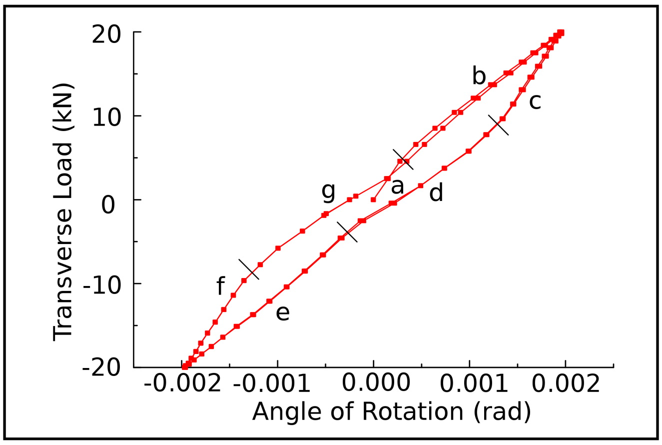


**Figure 3.** Angle of rotation-load curve.

and the axis of flange cylinder is along Z direction, thus the angle of rotation taken into consideration is rotation around X direction. Figure 3 presents the angle of rotation - load curve under the amplitude of harmonic load of 20,000 N. The curve is clearly a hysteresis loop like a willow leaf. The two cycles in the curve are less distinct. In the initial stage of loading, the stiffness decreases suddenly as soon as the load reaches the value of 6,000 N. The stiffness before decrease is defined as initial stiffness, and the one after is defined as changed stiffness.

The angle of rotation-load curve, which is nonlinear, is divided into 7 linear stages, as shown in Fig. 3. Stage $a$ is the process of initial loading, in which the angle of rotation increases linearly along with the increase of load. The sudden change of stiffness occurs at the junction of stage $a$ and $b$. This phenomenon is consistent with the experimental result in the reference;[20] therefore, the numerical calculation in this paper is proved credible. The angle of rotation and the load reach their maximum at the end of stage $b$. In stage $c$, which is the beginning of the unloading process, the stiffness of the joint is the same as the initial stiffness in stage $a$. Stage $d$ is also the process of unloading and stage $e$ is the process of loading in the opposite direction to the initial loading. The curves in stage $d$ and $e$ are approximately linear. Stage $f$ is the beginning of the unloading process the same as stage $c$, and stage $g$ is the unloading process the same as stage $d$. After Stage $g$ comes the second cycle, which starts from stage $b$ but not $a$. The entire curve excluding stage $a$ is symmetrical about the origin. The stiffness values of stage $a$, $c$, and $f$ are almost identical to the initial stiffness. The stiffness values of stage $b$, $d$, $e$, and $g$ are similar to the changed stiffness. These different kinds of stiffness values, the initial stiffness and the changed stiffness, display the shape of hysteresis loop.

## 3. MECHANISM OF HYSTERESIS

The stiffness of the joint consists of two parts; one is the stiffness of ring flange $k_1$, and the other is the stiffness of the snap $k_2$. Therefore, the total stiffness is

$$k = k_1 + k_2; \tag{1}$$

When the joint is bending, the value of $k_1$ remains constant on the condition of ignoring the material nonlinearity and large deformation; however, the value of $k_2$ varies with the con-

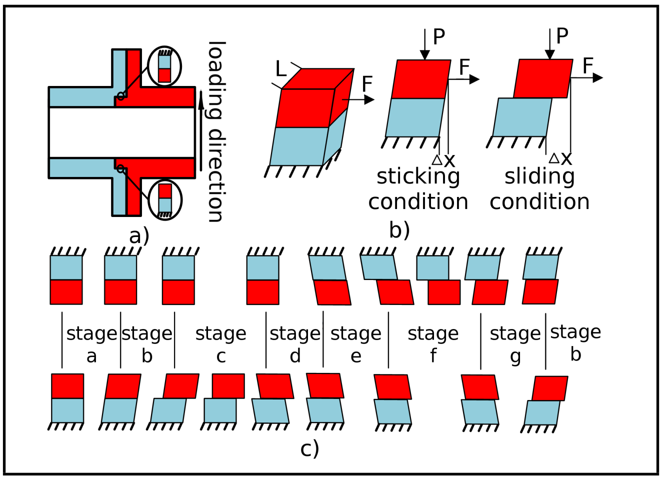


**Figure 4.** a) two ideal ICEs at the upside and downside, b) a ICE and its different status, c) sketch of deformation and slipping of two ideal ICEs in different stages.

tact status of the snap's interface. Thus, the total stiffness $k$ changes.

Assume that at the interface of the snap exist an infinitesimal contact element (ICE), as shown in Fig. 4a and Fig. 4b. The external forces of ICE are the pressure $P$ and the tensile force $F$ caused by the bending of joint. $\Delta x$ represents the sum of elastic deformation and slipping distance under the load of tensile force $F$. If tensile force $F < \mu P$ ($\mu$ is the coefficient of slipping friction of the interface), the ICE will be in sticking condition, on which there is no slipping in the interface and $\Delta x$ will only consist of elastic deformation. In this case, the required tensile force is:

$$F = GL\Delta x; \tag{2}$$

where, $G$ is the shear modulus and $L$ is the width of ICE as shown in Fig. 4b.

According to Coulomb's law, once the tensile force reaches the condition:

$$F = GL\Delta x > \mu P; \tag{3}$$

The interface begins to slip. If the slipping is at low speed, the tensile force can be written as

$$F = \mu P. \tag{4}$$

The result can be obtained from Eq. (3) that:

1. When the interface begins to slip, the bigger $G$ is, the smaller $\Delta x$ is.

2. The smaller $P$ and $\mu$ are, the smaller the tensile force $F$ is, which starts the slipping.

It can be seen from Eq. (3) that the tensile force $F$ remains constant no matter how $\Delta x$ changes, once the interface begins to slip.

Assume that at the upside and downside of the snap exist two ideal ICEs, which represent the contact status of the majority parts of interface at each side, as shown in Fig. 4a. In this section, the sticking, which always means deformation of ICE, and slipping of ideal ICEs are analysed based on the different characteristic of the joint's deformation in the 7 stages (as shown in Fig. 4c).

In stage $a$, the upsides of two pieces of flange plates are subject to compression under the upward load; the downsides of the flange plates are subject to tension and tend to be separated. There is no deformation and slipping in the upside ideal ICE, because two pieces of flange plates are close to each other; and only elastic deformation is occurred in the downside ideal ICE because of the smaller load in the initial loading stage $a$. With the load increasing in stage $b$, the downside ideal ICE begins to slip.

Stage $c$ is the stage of unloading, in which the elastic deformation of the downside ideal ICEoccurred in stage $a$ is restored firstly, and elastic deformation is occurred subsequently in the opposite direction.

In stage $d$, the downside ideal ICE slips again. In stage $d$, the contact statuses of upside and downside of the flange change. The upsides of the two pieces of flange plates begin to be subject to tension and the elastic deformation of upside ideal ICE occurs.

After stage $e$, the upside ideal ICE experiences three stages in sequence: slipping (stage $e$), restoring elastic deformation and elastic deformation in the opposite direction (stage $f$), and slipping again (stage $g$).

In stage $g$, the contact statuses of upside and downside flange change again. After stage $g$, the next cycle begins from stage $b$, but not stage $a$, which is the initial loading stage existing only in the first cycle.

In summary, there is only elastic deformation of ideal ICE in stage $a$, $c$, and $f$; and the ideal ICEs experience slipping in stage $b$, $d$, $e$, and $g$. Though there is elastic deformation of ICE in the stage $d$ and $g$, slipping is the major characteristic in the two stages.

The contact statuses of the interface vary in different positions of the snap. Thus, the ideal ICE does not represent any specific contact statues of the whole interface, but only shows the general trend of slipping and elastic deformation of the upside and downside part of the snap.

In order to prove valid analysis of ideal ICE above, the accumulated slipping distance of all contact elements in the snap are extracted from the computational results of ANSYS. Figure 5 shows the variation of average slip distance along with the angle of rotation. The slope of curve represents the rate of the change of slipping distance. The higher rate means that more elements experience slipping as every element has almost the same speed. According to thespeed of slipping, the curve can be divided into 7 stages, which is corresponding to the 7 sages in Fig. 4c. As shown in Fig. 5, the slopes of curve in stage $a$, $c$, and $f$ are almost the same and relatively small. It means that more part of the interface is in the status of sticking than the one in stage $b$, $d$, $e$, and $g$, thus there is less slipping but more elastic deformation. The slopes of curve in stage $b$, $d$, $e$, and $g$ are almost the same and bigger than in stage $a$, $c$, and $f$. It means that the more part of the interface experiences slipping.

Consider an arbitrary position $i$ on the snap as shown in Fig. 6, and its displacement (including deformation and slipping) and load when the joint is bending are analysed.

When the angle of rotation of joint is $\varphi$, the displacement of ICE $i$ can be written as

$$\Delta x_i = \tan\varphi\,(r\sin\theta_i + r) \approx \varphi\,(r\sin\theta_i + r)\,; \tag{5}$$

where $r$ is the radius of the snap.

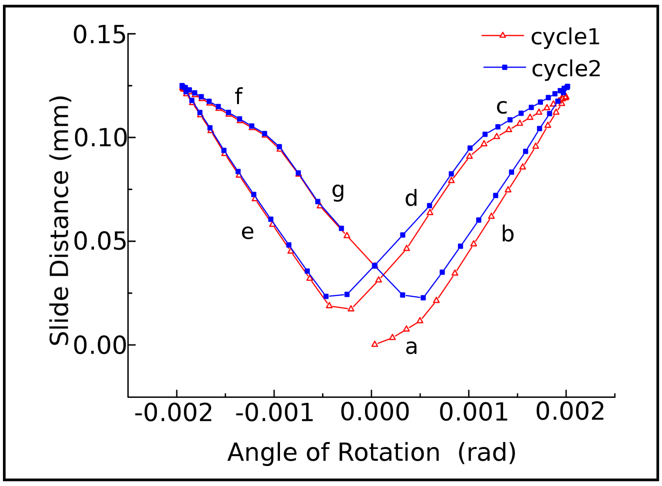


**Figure 5.** Average slip distance of all contact elements in the snap.

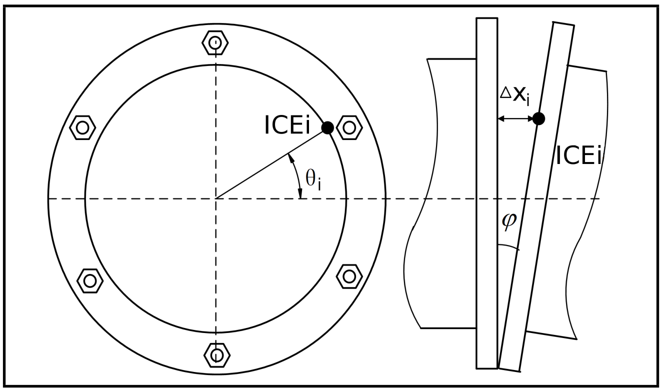


**Figure 6.** Position of ICE $i$.

According to Eq. (2) and (3), when ICE$i$ is in the status of sticking, the tensile force is

$$F_i = GL\Delta x_i. \tag{6}$$

When ICE$i$ is in the status of slipping, the tensile force is

$$F_i = \mu P_i. \tag{7}$$

Taking all ICEs of the snap in account, the bending moment which causes the angle of rotation $\varphi$ can be written as

$$M = \sum_{i=1}^{n} F_i \left(r \sin\theta_i + r\right); \tag{8}$$

where $n$ is the number of ICEs of the snap.

Assume that the amount of ICEs in the status of stick is $m$, the bending moment $M$ can be deducted by combining the three Eq. (6), (7), and (8) as

$$M = \sum_{i=1}^{m} GL\varphi \left(r \sin\theta_i + r\right)^2 + \sum_{i=m+1}^{n} \mu P_i \left(r \sin\theta_i + r\right). \tag{9}$$

The bending stiffness $k_2$ can be obtained by calculating the derivative of the bending moment

$$k_2 = \frac{dM}{d\varphi} = \sum_{i=1}^{m} GL \left(r \sin\theta_i + r\right)^2. \tag{10}$$

It can be seen from Eq. (10) that there is a positive correlation between bending stiffness $k_2$ and the value of $m$. That is, the higher the value of $m$ is, the bigger bending stiffness $k_2$ is; and the lower the value of $m$ is, the smaller bending stiffness $k_2$ is.

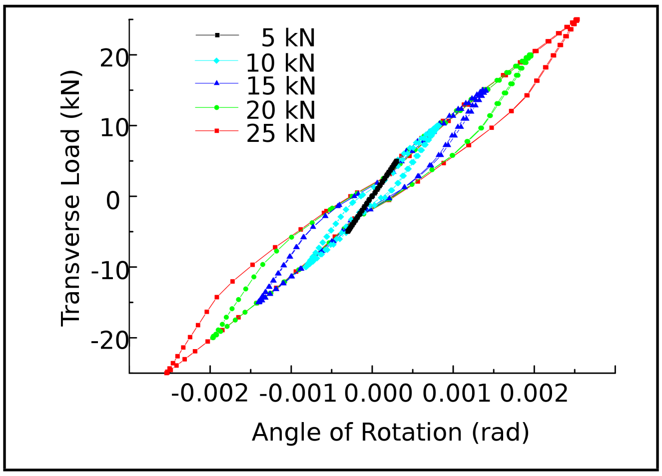


**Figure 7.** Angle of rotation-load curve under different loads.

According to the data in Fig. 5, there is less slipping but more elastic deformation in stage $a$, $c$, and $f$. Thus, the total stiffness is bigger than the one in stages $b$, $d$, $e$, and $g$, in which more part of the interface experiences slipping than in stage $a$, $c$, and $f$. The difference of stiffness in distinct stages causes the angle-loading curve to be a hysteresis loop in one cycle.

## 4. INFLUENCE OF THE JOINT'S PARAMETERS ON HYSTERESIS LOOP

The harmonic load of 5 kinds of amplitude (5 kN, 10 kN, 15 kN, 20 kN, 25 kN) is respectively applied to the finite element model with the interference fit of 0.06 mm to obtain the angle-loading curve, as shown in Fig. 7.

In Fig. 3, it is clearly shown that once the stiffness changes in the stage of initial loading, the curve is a hysteresis loop. In Fig. 7, four curves are hysteresis loops but one curve is not because the amplitude of load 5 kN is too small to make the stiffness change. In the four hysteresis curves, the value of the load which is required to make the stiffness change is almost the same, which is called $F_{CR}$ in this paper. When the amplitude of load is 5 kN, the entire curve is a line,with nothing nonlinear. The comparison of the four loop curves reveals that the bigger the amplitude of load is, the bigger the area of hysteresis loop is. For the same $F_{CR}$ in the four curves, the widths of hysteresis loops are the same. But the length of hysteresis loop increases with the growth of the amplitude of load, since the influence of material nonlinearity is ignored.

The 5 models with different contact characteristic in the snap are used to study the effect of interference on the hysteresis of joint, as shown in Fig. 8. It is clearly shown that the hysteresis loop is getting shorter and thicker when the interference increases. That is because the interference directly affects the pressure of contact interface, making it difficult to slip. Thus, the $F_{CR}$ is positive correlated to the interference. At the same time, bigger interference leads to higher value of stiffness, which results in the less angle of rotation. When the interference is 0 mm, there is no initial contact pressure in the snap. But tiny interference will appear with the deformation of joint under the transverse load. It is not easy to distinguish the change of stiffness due to the small contact pressure in the

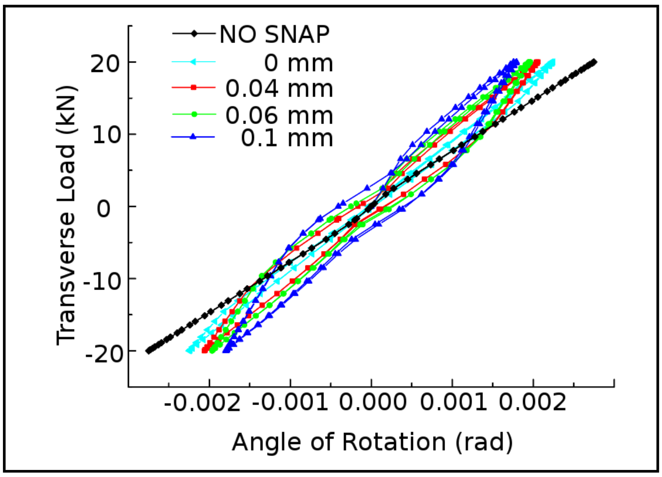


**Figure 8.** Angle of rotation-load curve of models with the different snap.

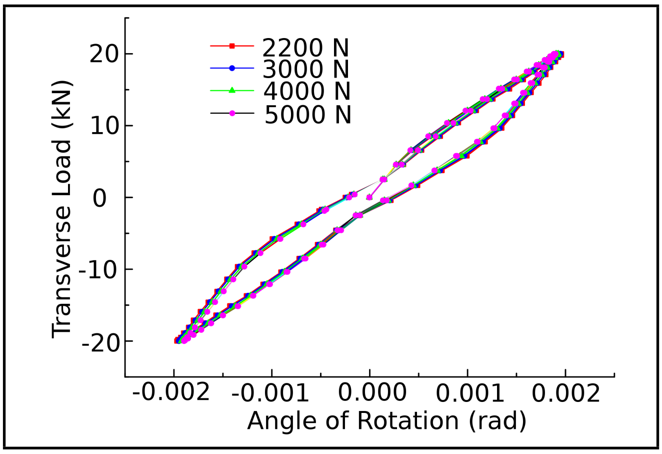


**Figure 9.** Angle of rotation-loading curve of models with different preload.

snap and the hysteresis loop is very thin. The curve of the model with no snap is completely a line, and the stiffness of the model with no snap is less than both the initial stiffness and the changed stiffness in the other four models. Thus, the snap has the effect of increasing the bending stiffness because of its interference in the contact interface.

Figure 9 shows the effect of preload on the hysteresis of the joint. The 4 cases of preload vary from 2200 N to 5000 N, in which the 4 curves almost coincide. This illustrates that the preload has little effect on the stiffness and hysteresis.

## 5. EFFECT OF HYSTERESIS ON VIBRATION

In the displacement-loading curve, the area of hysteresis loop presents the energy dissipation of the structure's vibration in one cycle. Thus, the structure with hysteresis will consume a large amount of energy during vibration for its high frequency of vibration.

### 5.1. Rotor Model with Flange Joint

In order to enhance the computing efficiency and retaining the characteristic of hysteresis, the joint of the rotor was modelled by three-dimensional finite element model, and the other parts are model by beam element based on Timoshenko theory(BEAM188). The two kinds of model are connected through constraint equations, as shown in Fig. 10a.

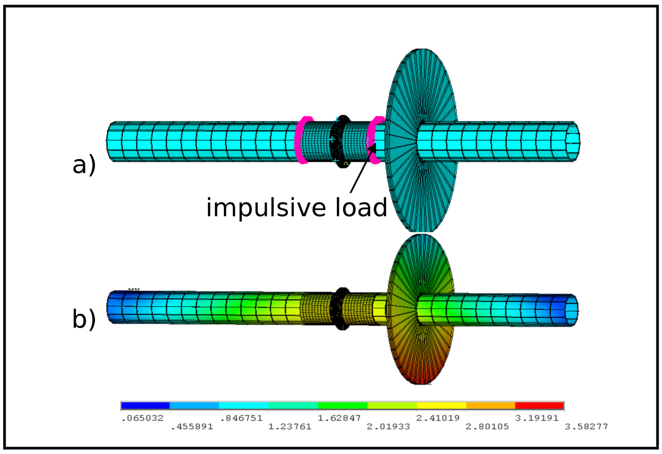


**Figure 10.** Rotor model with flange joint a) Finite element model, b) Vibration diagram.

In this charter, the effect of hysteresis on the attenuation of vibration is studied. For the general application for both rotor and stator, the gyroscopic effect of rotor is ignored. The left node of model is constrained in three directions (UX, UY and UZ), and the right node is constrained in two directions (UX and UY). Step-impulsive loading was applied to a node between the joint and the disk to simulate impulsive load. The full transient dynamic analysis is used to calculate during 0–1 s. 0–0.07 s is used to apply preload and 0.07 s–0.1 s is used to apply impulsive load. 0.1–1 s is used to calculate the response of rotor. The time step is 5s–4s, which is so short to capture the vibration frequency. Figure 10b is the vibration diagram of first order bending vibration which is excited by transverse load.

### 5.2. Time-domain Response

The vibration response of the node to which the impulsive load is applied is analysed to study the attenuation of amplitude. The slope of envelope curve of the vibration response curvesignifies the speed of attenuation. The two curves of vibration responses under different load are shown in Fig. 11. The free vibration is started at 0.1 s, and the initial amplitudes under load of 10 kN and 40 kN are 1.7 mm and 6.8 mm respectively. With the increase of time, the amplitudes of the two sets of calculated data attenuate obviously. But big distinction can be found in the speed of attenuation between the two sets of calculated data. The speed of attenuation before 0.2 s under the load of 10 kN is faster than the one after 0.2 s. And the speed before 0.4 s under the load of 40 kN is faster than the one after 0.4 s. It is evident from Fig. 11 that once the amplitude is attenuated to 0.3 mm, the speed of attenuation noticeably slows down. For this model, the amplitude of 0.3 mm is its critical amplitude in this paper. If the amplitude is bigger than the critical amplitude, the joint vibrates with the characteristic of hysteresis, which increase the dissipation of energy. Thus the amplitude will be attenuated to the critical amplitude rapidly. When the amplitude is equal to the critical amplitude, the stiffness of joint is linear and the joint vibrates with no characteristic of hysteresis. Thus the speed of attenuation noticeably slows down as the lack of energy dissipation of hysteresis. It is also clearly observed that the bigger amplitude is, the faster speed of attenuation is. Because the bigger amplitude leads to the bigger longitude of the hysteresis loop, it results in more dissipation of energy in one cycle.

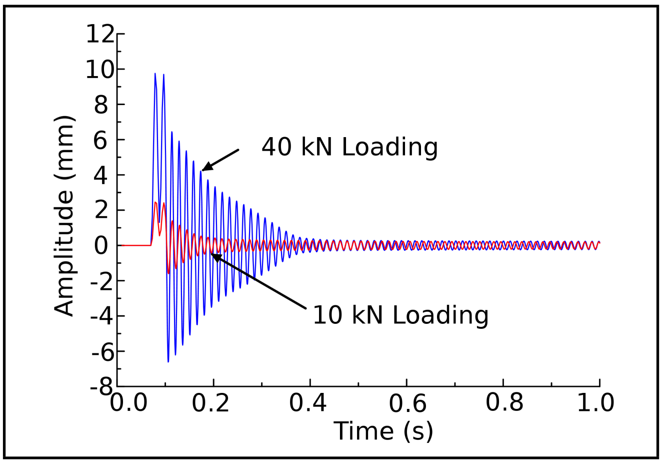


**Figure 11.** Time-domain response under different loads.

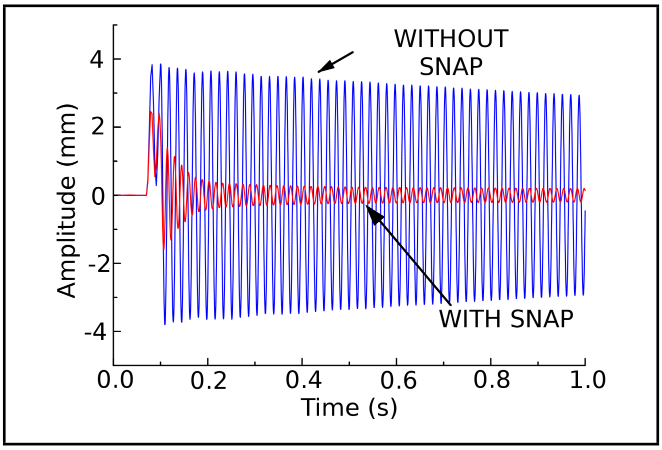


**Figure 12.** Influence of the snap on response.

The model which is without a snap is studied to compare the effect of the snap on the attenuation of amplitude. The two curves of free vibration responses under the load of 10 kN, which each other belong to the model with a snap and the model without a snap are shown in Fig. 12. Through comparing the changes of two curves, it is found that the initial amplitude of the model without a snap is obviously bigger than the one of the model with a snap because thestiffness of the joint with a snap is bigger and the speed of attenuation of the model without a snap is obviously slower for the lack of dissipation of energy. The model without a snap vibrates in the condition of big amplitude for the whole time.

The loads of 10 kN and 1.5 kN are applied to the model with the interference of 0.06 mm respectively to obtain its free vibration response. The two curves of the free vibration response are shown in Fig. 13. The initial amplitude of the set of 1.5 kN is obviously smaller than the one of 15 kN. In the whole process, the speed of attenuation remains low, in which there is no obvious change of the speed of attenuation. The amplitude of the set of 1.5 kN is so small that the whole process is in the stage of initial loading and there is no hysteresis in the whole vibration to consume energy.

The analyses above show that the speed of attenuation which is caused by the structural damping is very slow, but the amplitude of the model with a snap will be attenuated to the critical amplitude rapidly by the way of dissipation of energy. If the hysteresis characteristic is applied to the design of vibration suppression in aero-engine, compared to squeeze film damper,

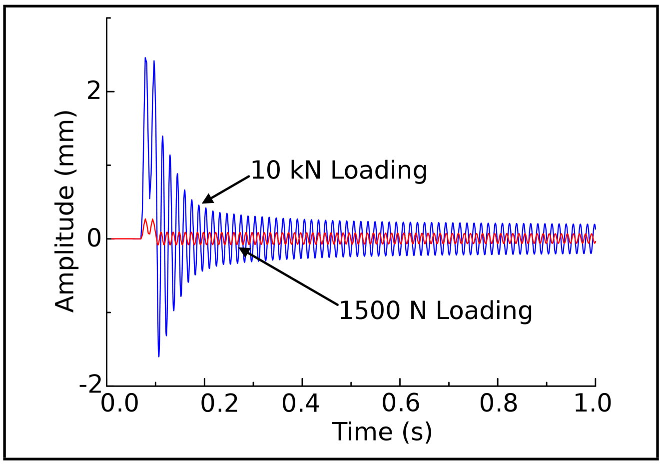


**Figure 13.** Influence of hysteresis.

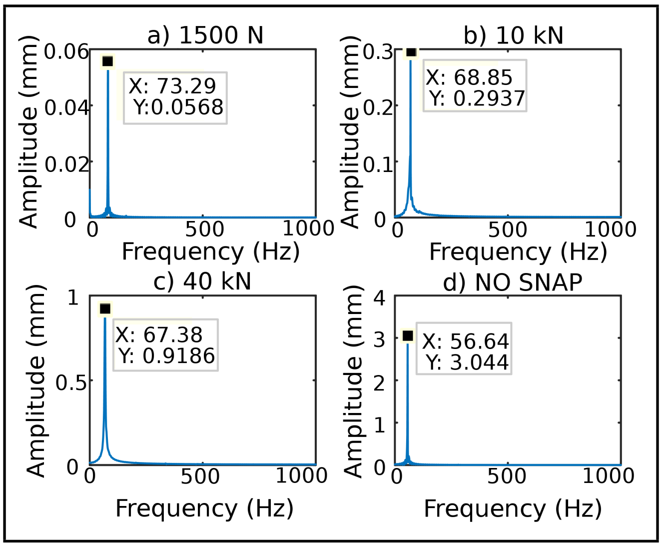


**Figure 14.** Frequency domain response.

the stiffness of joint is linear when the amplitude is below a certain value. Once the amplitude is above the certain value, the hysteresis appears and makes the amplitude fall down rapidly below the certain value.

## 5.3. Frequency Domain Response

The frequency response curves of four sets of calculated data are shown in Fig. 14. It can be found that the response frequency in Fig. 14d is smaller obviously than the other three sets because the lack of the snap causes the smaller stiffness. The Bottom of the response peaks in Fig. 14b and Fig. 14c, in which the hysteresis happens, are thicker than the two response peaks in Fig. 14a and Fig. 14d; There are more complex frequency components closed to the peak frequency in the former response peaks. The hysteresis is caused by the difference of stiffness in distinct stages which also cause this complex frequency components. The two sets of peak frequency in Fig. 14b and Fig. 14c are a little smaller than the one in Fig. 14a, this is because the model without hysteresis only experiences the stage $a$, and the model with hysteresis mainly experience the stage $b$, $d$, $g$, and $e$ whose stiffness is smaller than the one in stage a as shown in Fig. 3.

## 6. CONCLUSIONS

Based on FEM nonlinear numerical simulation, the nonlinear dynamic characteristic of the joint is discovered in this paper.

1. When the joint with a snap is under the certain transverse harmony load, the angle of rotation-loading curve presents the hysteresis characteristic, which is caused by the slipping of the contact interface in the snap.

2. The bigger the amplitude of load is, the bigger the area of hysteresis loop is. The bigger the value of interference is, the shorter and thicker of hysteresis loop is. The decrease in friction of the snap, which facilitates slipping, makes it easier for the hysteresis to appear.

3. When the model's amplitude is below a certain value (called critical amplitude in this paper), the bending stiffness keeps a constant. But when the amplitude is above the certain value, the hysteresis appears and makes the amplitude fall back quickly below the value.

4. When the hysteresis appears, the peak frequency is a little smaller and there are more complex frequency components around the peak frequency.

## REFERENCES


[1] Kattner, M. and Crisinel, M. Finite element modelling of semi-rigid composite joints, *Comput Struct*, **78** (1–3), 341–353, (2000). https://dx.doi.org/10.1016/S0045-7949(00)00064-X

[2] Mayer, M. H. and Gaul, L. Segment-to-segment contact elements for modelling joint interfaces in finite element analysis, *Mech Syst Signal Process*, **21** (2), 724–734, (2007). https://dx.doi.org/10.1016/j.ymssp.2005.10.006

[3] Kim, J., Yoon, J., and Kang, B. Finite element analysis and modeling of structure with bolted joints, *Appl Math Model*, **31** (5), 895–911, (2007). https://dx.doi.org/10.1016/j.apm.2006.03.020

[4] Canyurt, O. E. and Sekercioglu, T. A new approach for calculating the stiffness of bolted connections, *Proc Inst Mech Eng L-J Mater*, **230** (2), 426–435, (2015). https://dx.doi.org/10.1177/1464420715576557

[5] Wang, C., Zhang, D., Zhu, X., and Hong, J. Study on the Stiffness Loss and the Dynamic Influence on Rotor System of the Bolted Flange Joint, *ASME Turbo Expo 2014: Turbine Technical Conference and Exposition*, Montreal, Canada, (2014). https://dx.doi.org/10.1115/GT2014-26191

[6] Yao, X., Wang, J., and Zhai, X. Research and application of improved thin-layer element method of aero-engine bolted joints, *Proc Inst Mech Eng G-J A E*, **231** (5), 823–839, (2017). https://dx.doi.org/10.1177/0954410016643978

[7] Qin, Z., Han, Q., and Chu, F. Bolt loosening at rotating joint interface and its influence on rotor dynamics, *Eng Fail Anal*, **59**, 456–466, (2016). https://dx.doi.org/10.1016/j.engfailanal.2015.11.002

[8] Ibrahim, R. A. and Pettit, C. L. Uncertainties and dynamic problems of bolted joints and other fasteners, *J Sound Vib*, **279** (3–5), 857–936, (2005). https://dx.doi.org/10.1016/j.jsv.2003.11.064

[9] Luan, Y., Guan, Z., Cheng, G., and Liu, S. A simplified nonlinear dynamic model for the analysis of pipe structures with bolted flange joints, *J Sound Vib*, **331** (2), 325–344, (2012). https://dx.doi.org/10.1016/j.jsv.2011.09.002

[10] Schwingshackl, C. W. and Petrov, E. P. Modeling of Flange Joints for the Nonlinear Dynamic Analysis of Gas Turbine Engine Casings, *J Eng Gas Turb Power-T Asme*, **134** (12), 122504–122504, (2012). https://dx.doi.org/10.1115/1.4007342

[11] Schwingshackl, C. W., Di Maio, D., Sever, I., and Green, J. S. Modeling and Validation of the Nonlinear Dynamic Behavior of Bolted Flange Joints, *J Eng Gas Turb Power-T Asme*, **135** (12), 122504–122504, (2013). https://dx.doi.org/10.1115/1.4025076

[12] Gaul, L. and Lenz, J. Nonlinear dynamics of structures assembled by bolted joints, *Acta Mech*, **125** (1–4), 169–181, (1997). https://dx.doi.org/10.1007/BF01177306

[13] Bograd, S., Reuss, P., Schmidt, A., Gaul, L., and Mayer, M. Modeling the dynamics of mechanical joints, *Mech Syst Signal Process*, **25** (8), 2801–2826, (2011). https://dx.doi.org/10.1016/j.ymssp.2011.01.010

[14] Qin, Z., Yan, S., and Chu, F. Dynamic characteristics of launch vehicle and spacecraftconnected by clamp band, *J Sound Vib*, **330** (10), 2161–2173, (2011). https://dx.doi.org/10.1016/j.jsv.2010.06.011

[15] Van-Long, H., Jean-Pierre, J., and Jean-Franois, D. Behavior of bolted flange joints in tubular structures under monotonic, repeated and fatigue loadings I: Experimental tests, *J Constr Steel Res*, **85**, 1–11, (2013). https://dx.doi.org/doi.org/10.1016/j.jcsr.2013.02.011

[16] Iwan, W. D. *The Dynamic response of bilinear hysteretic systems*, California Institute of Technology, California, (1961).

[17] Argatov, I. I. and Butcher, E. A. On the Iwan models for lap-type bolted joints, *Int J Non-Linear Mech*, **46** (2), 347–356, (2011). https://dx.doi.org/10.1016/j.ijnonlinmec.2010.09.018

[18] Oldfield, M., Ouyang, H., and Mottershead, J. E. Simplified models of bolted joints under harmonic loading, *Comput Struct*, **84** (1–2), 25–33, (2005). https://dx.doi.org/10.1016/j.compstruc.2005.09.007

[19] Ouyang, H., Oldfield, M. J., and Mottershead, J. E. Experimental and theoretical studies of a bolted joint excited by a torsional dynamic load, *Int J Mech Sci*, **48** (12), 1447–1455, (2006). https://dx.doi.org/10.1016/j.ijmecsci.2006.07.015

[20] Shuguo, L., Yanhong, M., Dayi, Z., and Jie, H. Studies on dynamic characteristics of the joint in the aero-engine rotor system, *Mech Syst Signal Process*, **29**, 120–136, (2012). https://dx.doi.org/10.1016/j.ymssp.2011.12.001